Fermi Resonance in the Overtone Spectra of the CH Chromophore in $CHBr_3$. 2. Visible Spectra

Jan Davidsson,† Jonathan H. Gutow, Richard N. Zare,*

Department of Chemistry, Stanford University, Stanford, California 94305

Hans A. Hollenstein, Roberto R. Marquardt, and Martin Quack*

Laboratorium für Physikalische Chemie, ETH Zürich (Zentrum), CH-8092 Zürich, Switzerland
(Received: September 6, 1990)

Six new bands in the gas-phase overtone spectrum of $CHBr_3$ have been observed by using photoacoustic spectroscopy. These have been assigned to the Fermi resonance system between the CH stretching (ν_1) and CH bending (ν_4) modes. In addition, some combination bands involving ν_2 and ν_5 have been observed. These data combined with previous FTIR measurements (Ross, A.; Hollenstein, H.; Marquardt, R.; Quack, M. *Chem. Phys. Lett.* **1989**, *156*, 455) yield a total of 22 bands. We also present from the FTIR measurements some previously unassigned bands that are not associated with the stretch–bend Fermi resonance as well as some assignments for $^{13}CHBr_3$ in natural abundance. An analysis is made, using both band positions and band intensities, in the framework of the effective tridiagonal Hamiltonian and variational vibrational calculations using a normal coordinate and a curvilinear internal coordinate Hamiltonian. Anharmonic coupling constants ($k'_{sbb} \simeq 55$ cm^{-1}) and potentials for the CH stretching and bending modes are presented. We find that kinetic energy coupling alone does not account for the observed Fermi resonance interactions in the curvilinear internal coordinates used. Vibrational redistribution can be separated into different time scales with fast (~100 fs) energy exchange between the CH stretching and bending modes but slow decay (>1–2 ps) into other modes.

1. Introduction

In order to obtain a thorough understanding of intramolecular vibrational redistribution in polyatomic molecules on the femtosecond time scale[1] it is important to investigate systematically specific "chromophores" in the infrared spectrum, which can show the signatures of the underlying dynamics. A prominent example is the CH chromophore in CHX_3 molecules, for which we have previously shown that the Fermi resonance between CH stretching and bending modes is the dominant dynamical feature governing ultrafast redistribution.[2-5] Bromoform, $CHBr_3$, is expected to show a dynamical behavior similar to other CHX_3 systems. However, a first study of high overtone spectra of bromoform vapor by Manzanares et al.[6] could not establish evidence for the expected Fermi resonance. In a recent publication[7] (hereafter I) we have reported the infrared spectra of $CHBr_3$ and have presented conclusive proof for a Fermi resonance with an effective coupling constant k'_{sbb} of a strength similar to the one observed in other CHX_3 molecules.

The data set of Fermi resonance bands in $CHBr_3$ reported in (I) is particularly small (only 16 bands, including two bands in the visible from ref 6). Therefore, the determination of coupling constants and potential functions remained comparatively uncertain ($k'_{sbb} \cong 75 \pm 30$ cm^{-1}). The potential function in normal coordinates was only moderately well-defined, and the potential constants F_{sbb} and F_{ssbb} in internal coordinates were essentially undetermined, even in sign.[8-11]

From (I) we could predict that a substantial number of additional Fermi resonance bands should be observable in the visible overtone spectrum, particularly with improved techniques of photoacoustic spectroscopy.[12-14] We thus undertook the present investigation, which indeed allowed the observation and assignment of six new bands in the visible part of the overtone spectrum in addition to determining more accurately the positions of the 6_1 and 5_1 bands previously observed by Manzanares et al.[6] Our new results also include accurate measurements of the relative intensities of the 6_1 and 6_2 and the 5_1 and 5_2 components. With the new information available, it is possible to confirm our earlier predictions and to obtain a more accurate estimate of the effective coupling constant k'_{sbb} and of the potential and dipole functions governing the Fermi resonance spectra. We note that in the early

† Present address: Department of Physical Chemistry, University of Göteborg, and Chalmers University of Technology, S-41296 Göteborg, Sweden.

(1) Faraday Discussion on Intramolecular Kinetics. *Faraday Discuss. Chem. Soc.* **1983**, *75*, 1.
(2) Dübal, H. R.; Quack, M. *Chem. Phys. Lett.* **1980**, *72*, 342; **1981**, *80*, 439; *J. Chem. Phys.* **1984**, *81*, 3779.
(3) Baggott, J.; Chuang, M. C.; Zare, R. N.; Dübal, H. R.; Quack, M. *J. Chem. Phys.* **1985**, *82*, 1186.
(4) Segall, J.; Zare, R. N.; Dübal, H. R.; Lewerenz, M.; Quack, M. *J. Chem. Phys.* **1987**, *86*, 634.
(5) Lewerenz, M.; Quack, M. *J. Chem. Phys.* **1988**, *88*, 5408.
(6) Manzanares, C.; Yamasaki, I. N. L. S.; Weitz, E. *Chem. Phys. Lett.* **1988**, *144*, 43.
(7) Ross, A.; Hollenstein, H.; Marquardt, R.; Quack, M. *Chem. Phys. Lett.* **1989**, *156*, 455.
(8) Hollenstein, H.; Lewerenz, M.; Quack, M. *Chem. Phys. Lett.* **1990**, *165*, 175.
(9) Carrington, T.; Halonen, L.; Quack, M. *Chem. Phys. Lett.* **1987**, *140*, 512; *J. Chem. Soc., Faraday Trans. 2* **1988**, *84*, 1371.
(10) Quack, M. *J. Chem. Soc., Faraday Trans. 2*, **1988**, *84*, 1591.
(11) Halonen, L.; Kauppi, E. *J. Chem. Phys.* **1990**, *92*, 3278. This paper contributes neither new data nor assignments and claims incorrectly that the reevaluation of the data of ref 7 would allow the unambiguous determination of the anharmonic constants F_{sbb} and F_{ssbb} in internal coordinates. These authors arbitrarily fix $F_{ssbb} = 0$ or $F_{ssbb} = -aF_{sbb}$. Thus, they merely rephrase the original result of ref 7 concerning the correlation of F_{sbb} and F_{ssbb}. Their Hamiltonian models I and II are equivalent to effective Hamiltonians with $k'_{sbb} \simeq 73$ cm^{-1}, identical with the original result of ref 7. These authors (HK) also choose an unrealistically large CH bond length in their calculations. A different structural input and G matrix is the obvious reason why they could not reproduce the calculations of ref 7. We have been able to reproduce our earlier calculations with our previous rough estimate of the G matrix, which does not correspond to a realistic structure of bromoform. A thorough discussion of the structure of $CHBr_3$ as relevant to force constants is given in ref 8 and section 3.3 of the present paper. We have also checked (previously and again here) that the conclusions of ref 7 do not depend upon the particular G matrix used. We have reconfirmed, in particular, that the conclusions remain the same even with the unrealistic structure used by these authors (HK, $r_{CH} = 111$ pm), with which we have reproduced also their calculation using the original CHQ Hamiltonian. Similar observations are expected to apply to the further expansion of the Hamiltonian originally suggested in ref 10 and carried out in part by HK. The predictions of higher bands by HK are particularly poor for both band positions and intensities and do not go beyond ref 7.
(12) Chandler, D. W.; Farneth, W. E., Zare, R. N. *J. Chem. Phys.* **1982**, *77*, 4447.
(13) Crofton, M. W.; Stevens, C. G.; Klenerman, D.; Gutow, J. H.; Zare, R. N. *J. Chem. Phys.* **1988**, *89*, 7100.
(14) Davidsson, J.; Gutow, J. H.; Zare, R. N. *J. Phys. Chem.* **1990**, *94*, 4069.

0022-3654/91/2095-1201$02.50/0

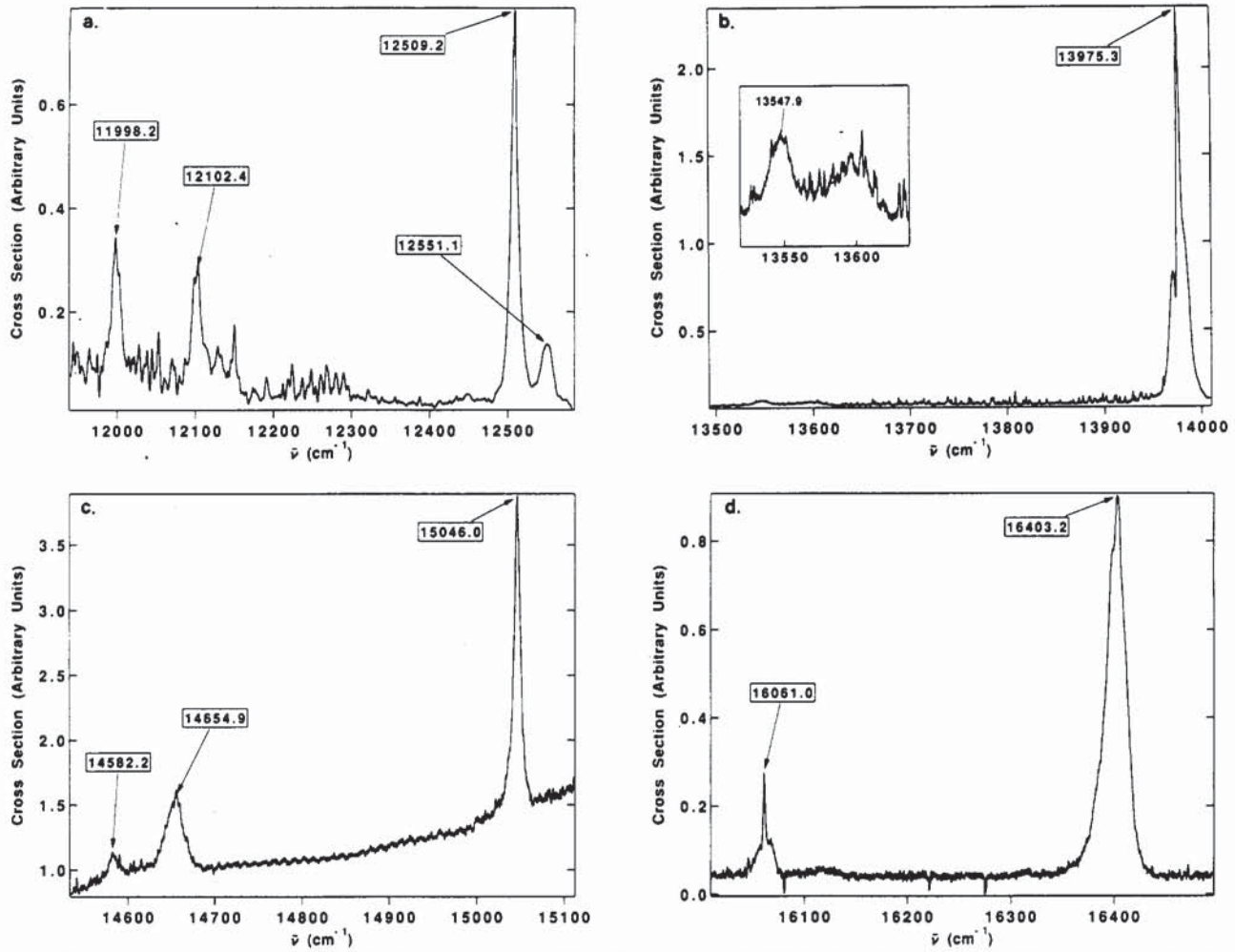

Figure 1. Survey of the gas-phase photoacoustic absorption spectra of the CH chromophore in $CHBr_3$ (sample pressure 0.55 kPa[2] experimental bandwith about 1 cm^{-1}, fwhm). (a) Range corresponding to $N = 9/2$ (the spectrum has been smoothed to remove noise). (b) Range of $N = 5$. (c) Range of $N = 11/2$. (d) Range of $N = 6$, see also text.

work on $CHBr_3$ infrared spectra a determination was made of vibrational fundamentals and force fields.[15-17] A report on overtone spectroscopy in the liquid included an observation of Fermi resonance.[18]

2. Experimental Section

The FTIR experiments have been described before.[2,7] In the present work we report some previously unassigned bands not belonging to the CH stretching–bending Fermi resonance system and four assignments for $^{13}CHBr_3$ in natural abundance.

For the photoacoustic experiments the $CHBr_3$ sample (Aldrich, 99%) was stored in a finger attached to the photoacoustic gas cell.[14] CaH_2 or NaH was placed in a second finger on the cell as a drying agent. The sample was degassed, removing also traces of ethanol, by multiple freeze–pump–thaw cycles. The cell was back-filled with xenon to bring the total pressure to 25–40 kPa. The $CHBr_3$ was then allowed to equilibrate to its vapor pressure (about 0.55 kPa at 295 K) before the spectra were recorded.

The photoacoustic spectra were obtained with an improved version[14] of our previous apparatus.[12,13] It was necessary to increase the sensitivity in order to record some of the very weak $CHBr_3$ combination bands. In the present experiments we used LD 700 laser dye pumped by the red lines of a Kr^+ laser (Spectra Physics 171) for the range 11 950–14 200 cm^{-1}. For higher frequencies the dyes were DCM, 14 500–15 400 cm^{-1}, and R6G, 15 800–16 500 cm^{-1}, pumped by an Ar^+ laser (Lexel 95) running multiline in the blue-green. The laser dyes were from Exciton and Lambda Physics. The laser beam was chopped at 1000–1200 Hz, so that the modulation was in resonance with the first longitudinal acoustic mode of the photoacoustic gas cell.

The photoacoustic spectrum was obtained by dividing the photoacoustic signal from the microphones (Knowles Electronics EA-3024) by the relative intracavity power. In addition, etalon fringes with a free spectral range of 3.23 cm^{-1} and the signal from a neon optogalvanic lamp were collected. All signals were digitized and stored on a computer. The etalon and optogalvanic signals were used to obtain absolute wavenumber assignments with an accuracy of about 0.5 cm^{-1}. The uncertainties in the wavenumber measurements arise mainly from the bandwidth of the laser system, about 1 cm^{-1}, fwhm.

Both the photoacoustic and the FTIR measurements were often made at or near the equilibrium vapor pressure of $CHBr_3$. Absolute band strength results measured under such conditions can only be considered to be rough estimates. The *relative* band strengths g_j within polyads (see definitions in section 3.4) should, however, be accurate to within a few percent of the stronger bands, which is important for the Fermi resonance analysis.

3. Results and Discussion

3.1. Survey of the Photoacoustic Spectra in the Visible Range. Figure 1 shows a survey of the photoacoustic spectra of $CHBr_3$ in the near-infrared and visible ranges. The spectral regions covered by the different dyes were 11 950–14 200, 14 500–15 400, and 15 800–16 500 cm^{-1}, which is fairly complete from 12 000–16 500 cm^{-1}. The highest frequency band observed in the FTIR

(15) Bürger, H.; Cichon, J. *Spectrochim. Acta* **1971**, *27A*, 2191.
(16) Shimanouchi, T. "Tables of Molecular Vibrational Frequencies"; NSRDS-NBS 39, Vol. 1, 1972, and references therein.
(17) Meister, A. G., Rosser, S. E., Cleveland, F. F. *J. Chem. Phys.* **1950**, *18*, 346.
(18) Fang, H. L.; Swofford, R. L. *J. Chem. Phys.* **1980**, *72*, 6382.

TABLE I: Experimental and Calculated Wavenumbers $\tilde{\nu}$ (in cm^{-1}) and Relative Intensities g for the CH–Chromophore Spectrum in $CHBr_3$

N_j	$\tilde{\nu}_{exp}$/cm^{-1}	footnotes	$\tilde{\nu}_{calc}$[k]/cm^{-1}	g_{exp}[g]	g_{calc}	$\tilde{\nu}_{ic}$[i]/cm^{-1}	$\tilde{\nu}_{nc}$[j]/cm^{-1}
$(1/2)_1$	1148.1	*a*	1152.9	1	1	1151.5	1154.0
1_2	2269.5	*a*, *b*	2276.0	(0.24)	0.003	2275.9	2279.1
1_1	3048.1	*a*, *c*	3049.7	(0.76)	0.997	3049.1	3048.1
$(3/2)_2$	3392.4	*a*	3396.8	(0.015)	0.005	3394.8	3395.7
$(3/2)_1$	4181.5	*a*, *d*	4182.7	0.985	0.995	4182.3	4182.0
2_3	4488.5	*a*	4487.8	(0.0002)	0.00001	4487.7	4482.0
2_2	5284.7	*a*	5285.4	0.06	0.006	5287.2	5287.9
2_1	5969.6	*a*, *e*	5972.1	0.94	0.994	5971.0	5970.3
$(5/2)_3$			5576.5		0.00004	5573.5	5559.5
$(5/2)_2$	6389.6	*a*	6385.6	0.09	0.012	6386.7	6385.7
$(5/2)_1$	7084.1	*a*	7085.7	0.91	0.988	7085.9	7083.9
3_3			7455.7		0.00006	7458.8	7454.5
3_2	8181.0	*a*, weak	8168.1	(0.036)	0.012	8170.5	8170.1
3_1	8766.0	*a*	8767.4	0.964	0.988	8765.9	8766.5
$(7/2)_2$			9248.1		0.024	9250.0	9248.7
$(7/2)_1$	9867.0	*a*	9862.3	(1)	0.976	9862.8	9859.7
4_2			10924.5		0.023	10926.5	10925.9
4_1	11429.9	*a*	11436.1	(1)	0.977	11434.5	11437.0
$(9/2)_3$			11343.9		0.0006	11345.5	11342.7
$(9/2)_2$	11998.2	*f*	11984.5	0.23	0.042	11985.3	11984.9
$(9/2)_1$	12509.1	*f*	12513.1	0.77	0.957	12514.1	11509.7
5_3			13012.3		0.0007	13012.4	13016.7
5_2	13548.0	*f*, *h*	13555.4	0.02	0.040	13555.8	13555.6
5_1	13975.3	*f*, *h*	13978.7	0.98	0.959	13977.8	13982.0
$(11/2)_3$			14038.0		0.002	14035.6	14042.3
$(11/2)_2$	14582.2	*f*	14595.3	0.076	0.074	14593.3	14594.6
$(11/2)_1$	15046.0	*f*	15039.4	0.924	0.925	15041.5	15034.6
6_4			15032.1		0.00002	15028.7	15043.5
6_3			15601.6		0.002	15595.6	15607.1
6_2	16061.0	*f*, *h*	16061.2	0.08	0.075	16059.3	16059.7
6_1	16403.2	*f*, *h*	16396.8	0.92	0.923	16398.0	16402.1

[a] FTIR data ref 7. [b] $^{13}CHBr_3$ assigned at 2258.8 cm^{-1}, predicted at 2261 cm^{-1} (ref 8). [c] $^{13}CHBr_3$ assigned at 3039.0 cm^{-1}, predicted at 3041 cm^{-1} (ref 8). [d] $^{13}CHBr_3$ assigned at 4169 cm^{-1}, predicted at 4167 cm^{-1} (ref 8). [e] $^{13}CHBr_3$ assigned at 5936.5 cm^{-1} (tentative), predicted at 5953 cm^{-1} (ref 8). [f] Photoacoustic data, this work. [g] Experimental intensities in parentheses are uncertain. [h] In the liquid, bands are observed at 10844, 11320, 12388, 13428, 13840, 15910, 16240 cm^{-1} (18). [i] $\tilde{\nu}_{ic}$ from the internal coordinate CHQ Hamiltonian. [j] $\tilde{\nu}_{nc}$ from the normal-coordinate Hamiltonian. [k] $\tilde{\nu}_{calc}$ is from the fit with the effective Hamiltonian.

TABLE II: Overtone and Combination Bands of $CHBr_3$ Not Assigned to the CH Stretching–Bending System

$\tilde{\nu}$/cm^{-1}	assignment	comments
2811.4	$1_2 + \nu_2$	*a*
3270	$1_1 + \nu_3$	*a*, A_1
3588.3	$1_1 + \nu_2$	*a*, A_1
3718.8	$1_1 + \nu_5$	*a*
3938	$(3/2)_2 + \nu_2$	
4136.5	$1_1 + 2\nu_2$	uncertain, weak
4723	$(3/2)_1 + \nu_2$	
5825	$2_2 + \nu_2$	
6652	$2_1 + \nu_5$	*a*, very weak
6930	$(5/2)_2 + \nu_2$	*a*
8719	$3_2 + \nu_2$	*a*
9437	$3_1 + \nu_5$	*a*, very weak
12102.4	$4_1 + \nu_5$	*b*
12551.1	$(9/2)_2 + \nu_2$	*b*, calc 12541
14654.9	$5_1 + \nu_5$	

[a] FTIR spectra (ref 7 and present work). [b] Photoacoustic spectra (this work).

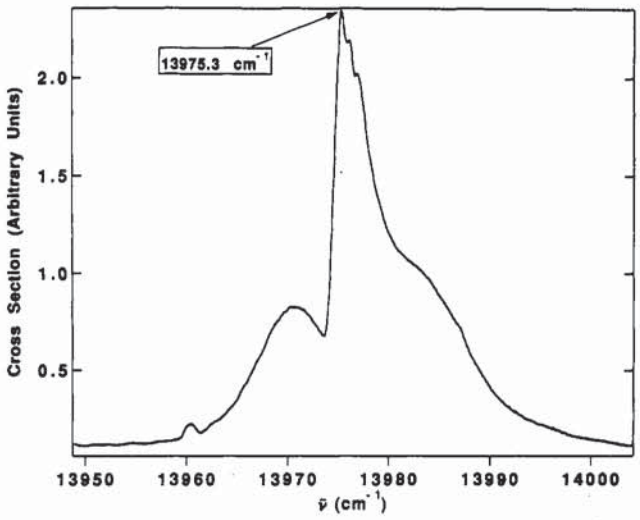

Figure 2. Detailed picture of the rovibrational envelope structure of the $N_j = 5_1$ band (experimental conditions as in Figure 1).

spectra is 4_1 at 11 430 cm^{-1}. FTIR spectra have been measured at higher frequencies, but the next strong band, $(9/2)_1$ near 12 509 cm^{-1}, is just too weak to be measured with certainty, even with almost 100-m optical path at saturation pressure. Although there is no overlap of the FTIR and photoacoustic measurements, they cover together essentially the complete spectral range from the far-infrared to the red part near 600 nm of the visible spectrum without important gaps. No significant absorption features beyond those presented in Figure 1 were found in the photoacoustic spectra. The four parts of Figure 1 correspond to one Fermi resonance polyad each, starting with $N = (9/2)$ and continuing to $N = 6$ (see the next section for a detailed discussion of the assignments). A magnification of the very weak 5_2 absorption is shown as an insert in Figure 1b. This is about the weakest feature measurable at the present detection limit of our photoacoustic spectrometer. Tables I and II summarize the measured band positions, including also intensity results. These tables give a complete list of all stronger bands. While the assignments are discussed in detail below we note that all bands, except a weak band at 12 551 cm^{-1}, find a definite assignment. Furthermore, all strong bands expected from the Fermi resonance CH chromophore model are, indeed, observed in the spectrum. Manzanares et al.[6] have previously reported the 5_1 and 6_1 overtones of bromoform. Their band positions differ from ours by about 10 cm^{-1}. Because we have calibrated against multiple Ne lines within a spectrum, we believe our frequencies in the photoacoustic spectra to be accurate to within the specified error of less than about 1 cm^{-1}. Of course, our data represent band maxima rather than

true band centers, as a rotational analysis could not be carried out.

In most cases the bands show well-defined envelopes, very similar to those observed in the FTIR spectra. Figure 2 shows a detailed plot of the 5_1 overtone at 13 975.3 cm^{-1}. One has a nicely defined P–Q–R structure for this parallel band. At low wavenumbers there is a sharp decrease in intensity whereas at the high-wavenumber side of the band there is a gradual, stepwise decrease. The latter arises from a sequence of hot bands, similar to the observations in the FTIR spectra of the 1_1 and 3_1 bands, reported before,[7] where the hot band structure is more clearly resolved. The weak band at 13 961 cm^{-1} may be a hot band, as also observed for some other bands in the FTIR spectra at the low-wavenumber side. The hot band structures and some further broad structures, particularly for the highest bands (e.g., 6_1), wash out the fine structures observed. Nonetheless, the envelopes of the stronger bands can generally be identified as being parallel (integer N polyads) or perpendicular (half odd integer N polyads) band types. This gives some clue to their assignments beyond the frequency and intensity of the bands.

3.2. Assignment of the CH Fermi Resonance Band Systems and Related Combinations. The assignment of the Fermi resonance band systems is straightforward, using the effective tridiagonal Hamiltonian defined by eqs 1 and 2.[2,7] The Hamiltonian

$$\tilde{H}^N_{v_s v_b l_b; v_s v_b l_b} = \tilde{\nu}'_s v_s + x'_{ss} v_s^2 + \tilde{\nu}'_b v_b + x'_{bb} v_b^2 + x'_{sb} v_s v_b + g'_{bb} l_b^2 \quad (1)$$

$$\tilde{H}^N_{v_s v_b l_b; v_s-1, v_b+2, l_b} = \tfrac{1}{2} k'_{sbb} [\tfrac{1}{2} v_s (v_b - l_b + 2)(v_b + l_b + 2)]^{1/2} \quad (2)$$

is block diagonal in the chromophore quantum number N (which equals $v_s + {}^1/_2 v_b$). The quantum states within the same block N constitute a polyad. States of the polyads are labeled N_j (j decreasing with increasing energy). For integer N one has parallel band structures, and for half odd integer N one has perpendicular band structures. The effective Hamiltonian $\tilde{\mathbf{H}}$ is diagonal in the vibrational angular momentum quantum number l_b (0 for integer N, 1 for half odd integer N). There are six adjustable parameters ($\tilde{\nu}'_s$, $\tilde{\nu}'_b$, x'_{ss}, x'_{sb}, x'_{bb}, g'_{bb}, in conventional spectroscopic notation) that define the diagonal structure of the effective Hamiltonian and one adjustable parameter (k'_{sbb}) that defines the off-diagonal structure and the strength of the Fermi resonance. Column "$\tilde{\nu}_{calc}$" in Table I presents the calculated wavenumbers from this Hamiltonian after least-squares adjustment of the parameters to the assigned bands. It turns out that a meaningful adjustment of all parameters to band positions alone is not possible, in spite of the much increased data set compared to ref 7. For instance, the root mean square deviation for systematic fits with values of k'_{sbb} ranging from 50 to 100 cm^{-1} varies only between about 6.2 and 6.5 cm^{-1}, well within some of the experimental and theoretical uncertainties. Therefore, it is crucial to include intensity information in the fits. In this context our new, accurate result for the relative intensities of the 6_1 and 6_2 pair and, to a lesser extent, $(11/2)_1$ and $(11/2)_2$ are most important. In these polyads the intensity redistribution by the Fermi resonance gives a significant intensity to the weaker band, which can thus be taken as the dominant signature of the Fermi resonance in $CHBr_3$. For the lower polyads the redistribution is much less significant and the intensity of the weaker bands 1_2 and 2_2, for instance, cannot be described by the Fermi resonance alone. We have thus set k'_{sbb} to 55 cm^{-1}, which describes well the intensity distribution in the highest polyads. This result is somehwat lower than our previous estimate, but well within the error limits previously stated (75 ± 30 cm^{-1}).[7] If k'_{sbb} is substantially changed from 55 cm^{-1}, the intensity ratios of the high polyads are much less well described (for instance, $g(6_1):g(6_2) = 0.76:0.22$, for $k'_{sbb} = 100$ cm^{-1}, which thus falls outside the acceptable range (see section 3.4). Table III summarizes the effective Hamiltonian parameters from this fit and some further ones to be discussed in more detail below.

Although most absorption bands in the near-infrared and visible regions can be assigned to the CH stretching–bending Fermi resonance system, a few remaining bands can be assigned to combinations with other fundamentals summarized in Table IV.

TABLE III: Parameters of the Effective Hamiltonian of the Fermi Resonance in $CHBr_3$

	experiment (this work)			ic		ref 7	
	a	*b*	nc[c]	*d*	*e*	fit 2[f]	fit 4[g]
$\tilde{\nu}'_s/cm^{-1}$	3111.6	3110.9	3111.1	3112.5	3119.6	3110.3	3111.3
$\tilde{\nu}'_b/cm^{-1}$	1154.1	1153.5	1155.0	1154.2	1143.1	1148.3	1147.5
x'_{ss}/cm^{-1}	−63.9	−65.6	−64.1	−64.2	−66.8	−64.1	−64.2
x'_{bb}/cm^{-1}	−7.6	−6.1	−8.5	−7.6	−6.7	−5.9	−5.8
x'_{sb}/cm^{-1}	−21.8	−26.6	−19.7	−21.4	−15.4	−18.0	−16.6
g'_{bb}/cm^{-1}	6.4	3.6	3.2	4.3	3.7	4.5	3.3
$\lvert k'_{sbb}\rvert/cm^{-1}$	55	100	55	55	55	63.1	54.4
d_{rms}/cm^{-1}	6.3	6.5	6.7 (6.6)	5.5 (1.7)	20.2 (3.2)	1.65	4.35

[a] Direct fit to 22 experimental bands fixing $\lvert k'_{sbb}\rvert = 55$ cm^{-1} to reproduce the relative band strengths of high polyads (see text). The parameters are rounded to one digit after the decimal point from those that give $\tilde{\nu}_{calc}$ in Table I. d_{rms} is the root mean square deviation. [b] Direct fit to 22 experimental bands, fixing $\lvert k_{sbb}\rvert = 100$ cm^{-1}, which gives, however, a poor prediction of intensities in high polyads (see text in section 3.2). [c] Fit to 22 experimental bands using the normal-coordinate Hamiltonian of ref 5 and transforming to tridiagonal form as described there. The d_{rms} in parentheses gives the error in the transformation, the other with respect to the experiment. k_{sbb} fixed (see footnote *a*). [d] Fit using the internal coordinate Hamiltonian of ref 9 and transforming to tridiagonal form (see also footnote *c*). [e] Fit using the internal coordinate Hamiltonian with the constraint $F_{sbb} = F_{ssbb} = 0$ (see section 3.3). From intensity redistribution and free floating of k'_{sbb} this would predict a very strong resonance ($k'_{sbb} \cong 100$ cm^{-1}). [f] Fit 2 of ref 7 to 16 bands (using the effective Hamiltonian). [g] Fit 4 of ref 7 to 16 bands (using the normal-coordinate Hamiltonian of ref 5 and transforming to tridiagonal form).

TABLE IV: Summary of Fundamentals of $CHBr_3$

fundamental	Γ	$\tilde{\nu}/cm^{-1}$	description	refs and notes
ν_1	A_1	3047.	CH stretch	this work, *a*
ν_2	A_1	542.6	CBr_3 sym stretch	*b*
ν_3	A_1	223.2	CBr_3 "umbrella"	*b*
ν_4	E	1146.5	CH bend	this work, *a*
ν_5	E	668.8	CBr_3 deg stretch	*b*
		669 ± 3		*d*
ν_6	E	155	CBr deg deform	*c*

[a] From Fermi resonance evaluation $\tilde{\nu}'_s + x'_{ss}$ or $\tilde{\nu}'_b + x'_{bb}$ (see Table III and also Table I). [b] From Bürger and Cichon (ref 15), see also ref 16 (vapor spectrum). [c] From IR spectrum of the liquid (ref 15) and Raman spectrum of the liquid (ref 17). See also ref 16 and references quoted there. [d] This work, new FTIR measurement at 0.1 cm^{-1} resolution (in the vapor), giving a broad contour, which only allows for a rough estimate of the band center (but superior to previous exptl. results). Note that $3\nu_3$ is expected at 669 cm^{-1}. There is a second band at 694 cm^{-1} ($\nu_2 + \nu_6$ according to ref 15).

The combination bands are shown in Table II. The list of strong bands in the near-infrared region in Table II is complete, whereas in the mid-infrared region a variety of combinations occur, as usual, not all of which are reported in Table II. The only prominent combinations in the near-infrared region are between the CH Fermi resonance system and the CBr_3 stretching vibrations ν_5 and ν_2. The situation is very similar to the one observed in CHD_3 and CHF_3 and has been discussed in great detail in refs 2–5. The relatively weak band at 12 551 cm^{-1} at the high-frequency side of the much stronger $(9/2)_1$ at 12 509 cm^{-1} might be caused by a local resonance perhaps with $(9/2)_2 + \nu_2$ expected around 12 541 cm^{-1}. This would lead to a small correction in the position of $(9/2)_1$. Another less likely possibility is that of a hot band. The strong bands in the high-overtone spectrum are thus all assigned.

3.3. Effective Hamiltonian and Potential Parameters in Internal and Normal Coordinates. The effective Hamiltonian parameters can be related approximately to properties of the anharmonic potential which couples the CH stretching and bending modes. This can be achieved either by means of a treatment in normal coordinates[5] (LQ Hamiltonian) or by using

curvilinear internal coordinates.[9] The simplified treatment in internal coordinates (CHQ Hamiltonian) can be considered to be a crude approximation to the more accurate normal-coordinate treatment. Consequently, we shall treat these briefly together, in order to obtain some insight into the anharmonic potential of bromoform.

The potential in the normal-coordinate subspace (Q_s, Q_b) is defined by[5]

$$\frac{V(\rho,\alpha)}{hc} = \frac{V(Q_s,Q_b)}{hc} = Dy^2 + \tfrac{1}{2}K_{\alpha\alpha}\alpha^2 + K_{\alpha^4}\alpha^4 + K_{\rho\alpha\alpha}\left[\frac{y}{a}\right]\alpha^2 + K_{\rho\rho\alpha\alpha}\left[\frac{y}{a}\right]^2\alpha^2 \quad (3)$$

Here Q_s and $Q_b = (Q_{b_1}^2 + Q_{b_2}^2)^{1/2}$ are the mass-weighted normal coordinates for the CH stretching and degenerate bending (b_1, b_2) motions and are related to *polar normal coordinates* ρ and α in the same way as polar coordinates are related to Cartesian coordinates

$$\rho = [Q_b^2 + (Q_s + \rho_0)^2]^{1/2} - \rho_0 \quad (4)$$

$$\alpha = \arctan\left[\frac{Q_b}{Q_s + \rho_0}\right] \quad (5)$$

The radial coordinate ρ is replaced by a dimensionless coordinate

$$y = 1 - \exp(-a\rho) \quad (6)$$

This type of potential for the Fermi resonance has been extensively tested with ab initio calculations and experimental data.[5,19] For the final computation of the spectrum this potential is transformed to rectilinear coordinates expressed as a Taylor series in the coordinates $\tilde{y}$ and q_b, which are related to Q_s and Q_b by the equations

$$q_{s\text{ or }b} = 2\pi Q_{s\text{ or }b}\,(\omega_{s\text{ or }b}c/h)^{1/2} \quad (7)$$

$$\tilde{y} = 1 - \exp(-\tilde{a}q_s) \quad (8)$$

In the limit of small amplitudes this coincides with the traditional Taylor expansion of the potential, with coefficients $C_{s^n b^m}$ including the factorial term in front of $\tilde{y}^n q_b^m$. Many terms in the Taylor expansion must be retained, even though the potential in eq 3 contains only a few parameters. Eigenvalues and eigenfunctions are calculated variationally, using the exact expressions for the kinetic energy operator. The methods have been discussed extensively.[5,19]

The column $\tilde{\nu}_{nc}$ in Table I has been obtained in this way. The resulting Hamiltonian can be transformed to tridiagonal form by a similarity transformation[5] and in this way equivalent effective Hamiltonian parameters are obtained (column n.c. in Table III). By comparison with experiment column a in Table III, one sees that the effective Hamiltonian parameters are very stable with respect to the method of evaluation. Of course, the large uncertainty in k'_{sbb} cannot be removed and this parameter was again fixed at 55 cm^{-1} in order to reproduce the intensity data, as discussed in section 3.2. Table V summarizes the potential constants derived from the fits. The relatively large uncertainty in the Fermi resonance constant k'_{sbb} is reflected by a related uncertainty in some potential constants, and several acceptable results are presented, which were obtained by a systematic variation of $K_{\rho\rho\alpha\alpha}$ around the minimum in the root mean square deviation d_{rms} of the fits. It is seen that ω_s, x_s, and $K_{\alpha\alpha}$ are well determined, whereas K_{α^4}, $K_{\rho\alpha\alpha}$, and $K_{\rho\rho\alpha\alpha}$ are somewhat correlated, but at least approximately determined with some significance. With simple dipole moment models it is possible to predict both absolute and relative intensities. The best fit in column b of Table V gives also an accurate prediction of relative intensities in the important $6_1/6_2$ pair. The different sets of potential constants in Table V lead to rather similar effective Hamiltonians and also to a rather similar appearance of the graphical representation of the potential. This is shown for the example of the best fit potential in Figure 3a.

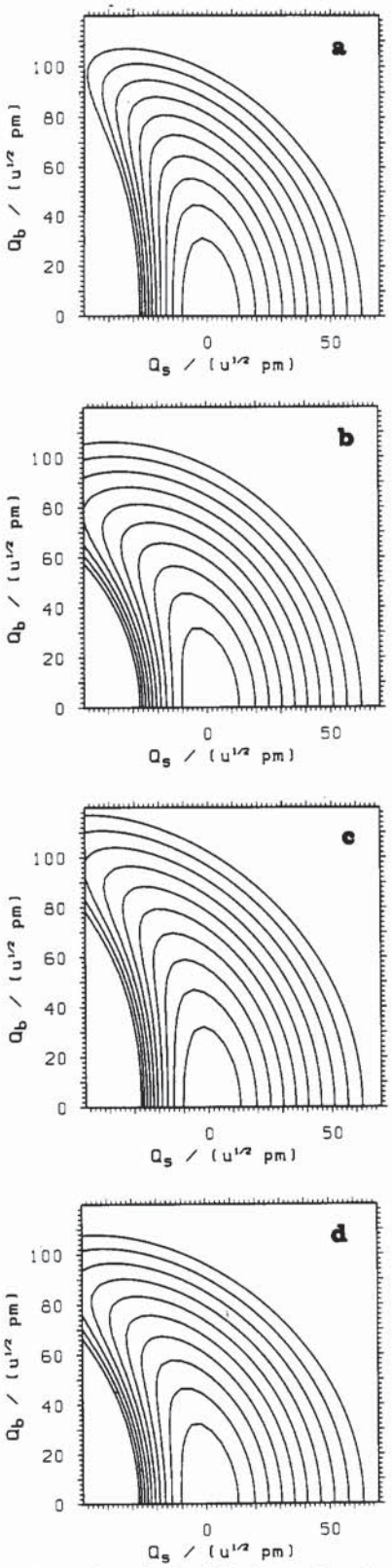

Figure 3. Potential surfaces for the CH chromophore Fermi resonance in reduced normal coordinates Q_s and Q_b. Equipotential lines are separated by $\Delta V/hc$ = 2000 cm^{-1} and cover the range to 20 000 cm^{-1}. (a) From best fit polar normal-coordinate Hamiltonian. (b) From best fit internal coordinate Hamiltonian equivalently represented in normal coordinates as described in the text. (c) As (b) but with F_{ssbb} = 300 000 cm^{-1} Å^{-2}, which gives a better description of intensities than (b). (d) As (b) but with $F_{sbb} = F_{ssbb} = 0$ (see text).

A more approximate, but conceptually attractive, model is based on the proposal of Sibert et al.[20] to formulate the Fermi resonance

(19) Dübal, H. R.; Ha, T. K.; Lewerenz, M.; Quack, M. *J. Chem. Phys.* **1989**, *91*, 6698.

TABLE V: Potential Constants for the Normal-Coordinate (LQ) Hamiltonian[a]

	b	c	d	e
ω_s/cm^{-1}	3194.4	3194.4	3193.7	3194.3
x_s/cm^{-1}	62.9	62.9	62.6	63.1
$K_{\alpha\alpha}$/cm^{-1}	45164	45312	45911	45047
K_{α^4}/cm^{-1}	−2203	−1784	−647.9	−3935
$K_{\rho\alpha\alpha}$/cm^{-1} u$^{-1/2}$ Å^{-1}	−47880	−52046	−64462	−35684
$K_{\rho\rho\alpha\alpha}$/cm^{-1} u^{-1} Å^{-2}	86142	95662	120000	60000
d_{rms}/cm^{-1}	6.7	6.7	9.1	7.0
D/cm^{-1}	40551	40560	40734	40426
a/Å^{-1} u$^{-1/2}$	1.932	1.932	1.922	1.935
ω_s/cm^{-1}	3194.4	3194.5	3193.7	3194.3
x_s/cm^{-1}	62.91	62.9	62.6	63.1
ω_b/cm^{-1}	1186.3	1184.3	1181.4	1195.9
C_{sbb}/cm^{-1}	181.3	171.4	140.5	208.6
C_{ssbb}/cm^{-1}	−73.9	−69.7	−57.5	−85.7

[a] The upper half of the table is sufficient to determine the potential, the constants in the lower half give the equivalent Morse parameters D and a, related to x_s and ω_s in the usual fashion and the constants ω_s, x_s, ω_b, C_{sbb}, and C_{ssbb}, which define the first few constants of the Taylor expansion in rectilinear coordinates (many more are important, see text and ref 5). ρ_0 is fixed at 1.031 u$^{1/2}$ Å everywhere. [b] d_{rms} is the root mean square deviation of the fit to 22 experimental bands, best fit result, used for $\tilde{\nu}_{n.c.}$ in Table I. The basis set is 17 stretching × 18 bending functions. A linear dipole function predicts $g(6_1):g(6_2)$ = 0.93:0.067 with this fit, in good agreement with experiment. [c–e] Results close to best fit (see text).

problem in curvilinear internal coordinates in such a way that most (or perhaps all) of the Fermi resonance coupling is derived from the kinetic energy operator in these coordinates. As discussed in ref 2, this simply leads to a *reinterpretation* of the Fermi resonance coupling parameter k'_{sbb} in terms of kinetic energy coupling, to the extent that this description is accurate. Quantitative formulations of the Hamiltonian for CHX_3 molecules (CHQ Hamiltonian) have shown, however, that in general both some kinetic and potential energy couplings are important,[9,19] with the notable exception of $CHBr_3$, for which our first, very limited data set allowed an interpretation by kinetic energy coupling only.[7,8] The present data should provide a more stringent test of this assumption.

The potential in standard internal curvilinear coordinates (index ic) is written as[9]

$$V = V_o + V_c \tag{9a}$$

$$\frac{V_c(r,\theta)}{hc} = \frac{1}{2a_{ic}}F_{sbb}y_{ic}\theta^2 + \frac{1}{4}[a_{ic}^{-2}F_{ssbb} + a_{ic}^{-1}F_{sbb}]y_{ic}^2\theta^2 \tag{9b}$$

$$\frac{V_o}{hc} = D_{ic}y_{ic}^2 + \frac{1}{2}F_{bb}\theta^2 + \frac{1}{24}F_{bbbb}\theta^4 \tag{9c}$$

$$y_{ic} = 1 - \exp(-a_{ic}r) \tag{9d}$$

We make use again of the Morse coordinate, now in internal coordinates, y_i, with the CH displacement coordinate $r = r_{CH} - r_{e(CH)}$. The angle θ is defined in the usual way[9] and is best visualized by the approximation $\theta \simeq (1.5)^{1/2}\Theta$, where Θ is the polar angle of r with respect to the C_3 symmetry axis. For exact relations see ref 19. In this model the expansion for the kinetic energy operator is only approximate,[9,10] which is a drawback of the model. The potential consists of a separable part V_o and a coupling term V_c with the cubic and quartic anharmonic force constants F_{sbb} and F_{ssbb}. These *cannot be associated with* the strength of the Fermi resonance, which is present even if $F_{sbb} = F_{ssbb} = 0$, in this model. Eigenfunctions and eigenvalues are calculated variationally. Details have been described elsewhere.[9,19]

Table VI summarizes the results of the least-squares adjustments of the potential constants of the CHQ Hamiltonian to the 22 experimental band positions. In spite of the much increased size of the data set, we confirm our earlier finding that the anharmonic constants F_{sbb} and F_{ssbb} cannot be uniquely determined from experiment. The root mean square deviation in systematic fits is almost constant and multiple acceptable solutions can be found with even variation of the *sign* of F_{ssbb} and F_{sbb}. F_{sbb} can be somewhere between −60 000 and +30 000 cm^{-1} Å^{-1} and F_{ssbb} varies in a correlated way between −300 000 and +300 000 cm^{-1} Å^{-2}. The anharmonic constants in internal coordinates thus remain largely undetermined. However, with our larger data set we can rule out a solution with $F_{sbb} = F_{ssbb} = 0$, which would correspond to the original suggestion of Sibert et al.[20] for the origin of the Fermi resonance. With the old data set and this simple model an acceptable root mean square deviation $d_{rms} \simeq 5$ cm^{-1} was obtained.[8] With the new, larger data set we have $d_{rms} \simeq 20$ cm^{-1} when $F_{sbb} = F_{ssbb} = 0$, which does not fall in the acceptable range, even when allowing generously for experimental and theoretical uncertainties. The pure kinetic energy coupling model[20] of the Fermi resonance can thus be ruled out for all CHX_3 molecules that we have investigated.[2-5,7-9,19] It may be noted that the pure kinetic energy coupling model predicts much too strong a resonance with an enormous intensity redistribution (60:40 in the $6_1/6_2$ pair) corresponding to $k'_{sbb} \simeq 100$ cm^{-1}. This is additional evidence (beyond d_{rms}) against this model. The intensity ratio in the $6_1/6_2$ pair also favors the solutions with F_{ssbb} between +300 000 and +150 000 in Table VI. The situation is somewhat less clear here, and rather underlines the ambiguities. With a linear dipole function model (see section 3.4) $g(6_1):g(6_2)$ = 95:5 with F_{ssbb} = +300 000, rather close to experiment, whereas for the "best d_{rms}" fit this would be 76:21, with F_{ssbb} = −244 000. If a choice had to be made, we would give more weight to the intensity fit than to d_{rms} and therefore prefer a large, positive F_{ssbb}.

A further uncertainty in the potential constants for the internal coordinates arises from the dependence upon the structural parameters assumed in the calculation.[7] The structure of $CHBr_3$ has been determined repeatedly by both microwave spectroscopy and electron diffraction methods.[21-23] None of these determinations provides a definite equilibrium geometry for $CHBr_3$. There is considerable uncertainty in the C–H bond distance r_{CH}. This quantity, however, is most important for the force constants F_{bb}, F_{sbb}, and F_{ssbb}. These are derived from spectral data by using the internal coordinate Hamiltonian, and they depend substantially upon the assumed value of r_{CH} (or, in general the **G** matrix including, to a lesser extent, other structural parameters). Bond distances r_{CH} quoted for $CHBr_3$ range from 106.8 to 111 pm, with sometimes differing definitions. Following our discussion in ref 8, we note that perhaps the best estimate of the CH bond distance can be derived from the correlations between bond distance and CH fundamental frequencies.[24] When we take the CH fundamental frequency corrected for Fermi resonance as derived here to be 3047 cm^{-1}, we calculate $r_{CH} \simeq 108.8$ pm from the correlations.[24] We note that, interestingly, $CHBr_3$ has the *highest* CH fundamental frequency in the series of CHX_3 molecules investigated in our work. We have taken a value of 109 pm in all our calculations reported here on $CHBr_3$. This is consistent with the value r_g = 111 pm derived in ref 23, because r_g is expected to be considerably larger than r_e.[25] Our new estimate is somewhat longer than the early microwave result.[21] The structural inputs and **G** matrices used in our calculations should, to some extent, be considered as nominal estimates used for deriving force constants. It is a simple matter to recalculate force constants using another **G** matrix input. Independent of this, the question of the structure of CHX_3 molecules and correlations with potential properties (frequencies and dissociation energies) remains interestingly open, as clearly demonstrated from our new, accurate

(20) Sibert III, E. L.; Reinhardt, W. P.; Hynes, C. *Chem. Phys. Lett.* **1982**, *92*, 455; *J. Chem. Phys.* **1984**, *81*, 1115, 1135.

(21) Williams, Q.; Cox, J. T.; Gordy, W. *J. Chem. Phys.* **1952**, *20*, 1524.

(22) (a) Hellwege, K. H., Hellwege, A. M., Eds. *Structure Data on Polyatomic Molecules*; Landolt Börnstein Tables Vol. II/7; Springer: Berlin, 1976; p 123. (b) Hirota, E.; Kuchitsu, K. *Ibid.* Vol. 15, Supplement to II/7 (New Series), 1987; p 1.

(23) Tamagawa, K.; Kimura, M. *Bull. Chem. Soc. Jpn.* **1979**, *52*, 2747.

(24) McKean, D. C. *Chem. Soc. Rev.* **1978**, *7*, 399.

(25) Kuchitsu, K.; Nakata, M.; Yamamoto, S. In *Stereochemical Applicatins of Gas Phase Electron Diffraction. Part A. The Electron Diffraction Technique*; Hargittai, I., Hargittai, M., Eds.; VCH Publishers Inc.: New York, 1988; p 227.

TABLE VI: Potential Constants for the Internal Coordinate (CHQ) Hamiltonian of $CHBr_3$

	a	*b*	*b*	*b*	*b*	*b*	*c*	*d*
D_{ic}/cm^{-1}	40036.4	40291.6	39843	39821	39784	39830.8	40120.3	38590.8
$a_{ic}/Å^{-1}$	1.8747	1.8706	1.8821	1.8814	1.8820	1.8804	1.8744	1.9065
F_{bb}/cm^{-1}	29430	30005	29691	29590	29506	29442	29184	28487.4
F_{bbbb}/cm^{-1}	−28167	−17118	−34512	−41678	−39503	−35001	−13919	−20000
F_{sbb}/cm^{-1} Å^{-1}	21680	−58875	−32477	−9743	67	10473	27150	0
F_{ssbb}/cm^{-1} Å^{-2}	−244100	300000	150000	0.	−70000	−150000	−300000	0
d_{rms}/cm^{-1}	5.5	7.3	6.8	6.2	6.0	5.7	7.9	21.2

[a] Best fit to 22 experimental data (d_{rms} is the root mean square deviation of the fit). Structural parameters used in the calculations m_H = 1.007825 u, r_{CH} = 109 pm, m_{Br} = 79.909 u, r_{CBr} = 193 pm, m_c = 12.0 u, <BrCBr = 110.8°; basis 12 × 24 (bending × stretching) functions, *g*-matrix elements: G_{rr} = 1.075 569 u^{-1}, $G_{\theta\theta}$ = 1.401 463 u^{-1} Å^{-2}, G_1 = −2.525 495 u^{-1} Å^{-3}, G_2 = 0.013 420 u^{-1} Å^{-4}, G_3 = 6.919 817 u^{-1} Å^{-4}. This calculation was used for $\tilde{\nu}_{ic}$ in Table I. Effective Hamiltonian parameters are given in Table III, column ic *d*). The intensity ratio is $g(6_1):g(6_2)$ = 76:21 in this fit. [b] Systematic variation of F_{ssbb} (fixed in each fit) to test the root mean square deviation d_{rms} as function of correlated changes of F_{ssbb} and other parameters (mostly F_{sbb}). The best fit of relative intensities in the important 6_1:6_2 pair occurs between F_{ssbb} = 300 000 and 150 000 with $g(6_1):g(6_2)$ = 95:5 and 87:12, respectively. F_{ssbb} = 0 already gives a poor prediction $g(6_1):g(6_2)$ = 81:17. [c] This result is obtained from systematic variation series with a constant assignment of eigenvalues. With a change of assignment a lower d_{rms} = 4.4 cm^{-1} (close to minimum) with the following constants in the order of the table is obtained 40174; 1.871; 29267; −16643; 28261, −300000 (fix). [d] F_{ssbb} = F_{sbb} = 0 fixed in the fit. A different assignment gives a very similar d_{rms}. In both cases the predicted resonance and intensity redistribution is much too strong ($k'_{sbb} \simeq 100$ cm^{-1}). There is an interesting avoided resonance crossing between 3_1 and 4_5 which was removed by setting F_{bbbb} = −20 000, which is close to but not exactly at best fit (see section 3.5).

result on the CH stretching frequency. There also remains the question of what G matrix is best to use in the CHQ Hamiltonian (from the equilibrium geometry or some average).

The problem of the dependence of the potential constants in internal coordinates upon the molecular structure assumed in the calculation does not arise in the normal-coordinate (LQ) Hamiltonian, because the potential is given in reduced coordinates, which can be transformed to geometries independently, making use of whatever knowledge is available on the molecular structure. One can approximately transform the potential in internal coordinates from Tabel VI to a potential in normal coordinates by taking the harmonic and anharmonic force constants in internal coordinates for the CH stretching and bending motions as derived here and the harmonic force field from the other internal coordinates as estimated in ref 15. The resulting anharmonic force constants in polar normal coordinates do not agree very well with those derived directly and also a too large effective coupling constant k'_{sbb} arises ($\simeq$120 cm^{-1}). The differences result in part from the large uncertainties in the case of $CHBr_3$, due to the limited data set. However, qualitatively the potentials have similar shapes as shown in the comparison of Figure 3, a, b, and c. The large curvature of the potential representation in reduced normal coordinates is the signature of the Fermi resonance. It can be described to some extent by the cubic constant C_{sbb}, which is identified with k'_{sbb} in early perturbation theory[26] and contains a substantial geometrical contribution just from the transformation from curvilinear internal coordinates to rectilinear normal coordinates. Quantitatively C_{ssbb} and many higher terms in the Taylor expansion are important.[5] Nevertheless C_{sbb} and much more so potential representations as those in Figure 3 give a good indication of the Fermi resonance coupling arising from *potential coupling alone* of the two modes involved (there is no kinetic energy coupling in these coordinates).

When the anharmonic potential is presented in curvilinear internal coordinates as shown in Figure 4, the "coupling appears weak", but this is misleading, because the coupling now arises largely through the kinetic energy operator. It is thus not useful to call F_{sbb} and F_{ssbb} "Fermi resonance constants", as they do not even give a qualitative indication of the strength of the Fermi resonance. But as we have discussed in detail elsewhere,[5,19] even C_{sbb} and C_{ssbb} can at most be related to the Fermi resonance *qualitatively*, but not quantitatively, as is also clear for $CHBr_3$ from Table V. For a quantitative treatment the complete set of anharmonic constants is needed and available from the polar normal-coordinate representation.

Finally, it may be useful to summarize some of the merits and disadvantages of the theoretical treatments of the Fermi resonance in reduced normal coordinates or internal coordinates. The internal

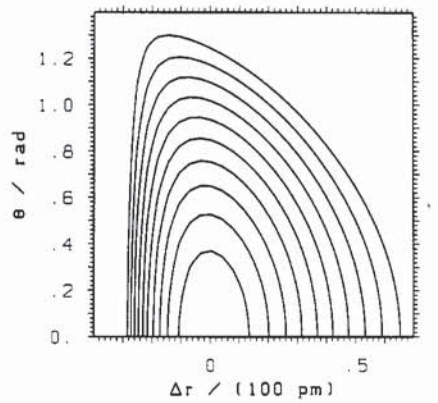

Figure 4. Potential surface for best fit CHQ Hamiltonian represented in internal coordinates (see discussion in text, equipotential lines are separated by $\Delta V/hc$ = 2000 cm^{-1}).

coordinate Hamiltonian has advantages because of numerical and, to a limited extent, conceptual simplicity. The drawback is the more approximate treatment of molecular motion and the approximate treatment of the kinetic energy operator, which is expanded in a series with unknown convergence.[10] While this is acceptable for some approximate treatments, it is unpleasant as a starting point for an exact treatment. With the present work we can rule out the simple idea of treating the Fermi resonance by kinetic energy coupling only in these curvilinear internal coordinates. Thus, much of the conceptual simplicity of this treatment is deceiving, because the complex interplay of potential and kinetic energy coupling in the model generates the Fermi resonance coupling in a way that is not at all transparent. Also, there is an awkward dependence of the force constants derived from the spectra upon the often unknown structural parameters of the molecule. None of these drawbacks occurs in the normal-coordinate treatment, which is a straightforward starting point for an exact treatment. However, the normal-coordinate Fermi resonance calculations are much more demanding numerically and this can be a serious drawback, particularly in least-squares adjustments, which may become both expensive and unstable. Thus, for many purposes it still seems useful to carry out both types of calculations.

3.4. Band Strengths and Dipole Functions. The experimental band strengths obtained in the present paper are only rough estimates and are therefore given without any error limits. They contain nevertheless some useful information, summarized in terms of the integrated cross section in Table VII:

$$G = \int \nu^{-1}\sigma(\nu)\, d\nu \qquad (10a)$$

$$\sigma = \frac{1}{Cl} \ln (I_0/I) \qquad (10b)$$

(26) Amat, G.; Nielsen, H. H.; Tarrago, C. *Rotation Vibration of Polyatomic Molecules*; Dekker: New York, 1971.

TABLE VII: Estimates of Absolute Band Strengths G for N = Integer Polyads of the CH Chromophore in $CHBr_3$

	G/fm^2					
N	expt	nc[a]	nc[b]	ic[c]	ic[d]	ic[e]
1	25000	25000	25000	71300	32000	51000
2	4700	980	2500	1900	3900	1470
3	120	59	7.1	83	270	54
4	2.9	4.8	0.34	5.2	23	2.7
5	0.18[g] (0.085)[f]		0.5	0.44	2.3	0.17
6	0.0081	0.064	0.0022	0.048	0.27	0.013

[a] Linear dipole model. [b] μ = const$(1 - e^{-\alpha Q_1})$. [c] $r_e/r_m = 0.459$, $m = 1.14$, $\mu_0 = 1$ D,[34] $r_e = 109$ pm (also below). [d] $r_e/r_m = 0.8$, $m = 1.3$, $\mu_0 = 1.7$ D. [e] $r_e/r_m = 0.562$, $m = 2.21$, $\mu_0 = 0.534$ D. [f] Ethane standard used in the photoacoustic experiments. [g] HD standard used in the photoacoustic experiments.

σ is the ordinary absorption cross section in the Beer–Lambert law, with the particle density C and the incident (I_0) and transmitted intensity (I), neglecting the small correction for stimulated emission. The integration is extended over each band N_j. G_{N_j} is related to the dipole transition moment[27]

$$G_{N_j} = 41.623755\left|\frac{\langle 0|\mu_z|N_j\rangle}{\text{debye}}\right|^2 \text{ pm}^2 \qquad (11)$$

μ_z is the z component of the dipole moment vector parallel to the symmetry axis (valid for the integer N polyads giving parallel bands). The polyad band strength G_N of the CH chromophore is obtained by summing

$$G_N = \sum_j G_{N_j} \qquad (12)$$

The relative band strengths for bands within a polyad are defined by

$$g_j = G_{N_j}/G_N \qquad (13)$$

The band strengths can be calculated with several simple one-dimensional dipole function models as also summarized in Table VII. As can be seen, the general trends are well represented, whereas details depend upon the dipole functions assumed. Although at present a definite result on the dipole function cannot be obtained, and in any case more accurate results would require retaining more than one dimension, it is of particular interest to consider the one-dimensional Mecke function (in internal coordinates here):[27-30]

$$\mu_z(r) = \mu_0(r_e)\left[\frac{r}{r_e}\right]^m \exp\left[\frac{r_e}{r_m}m\left(1 - \frac{r}{r_e}\right)\right] \qquad (14)$$

When we use this function to represent intensities, we find that the trend observed in the series CHF_3, $CHCl_3$, $CHBr_3$ is consistent with the position r_m of the maximum in the dipole function shifting from $r_m < r_e$ for CHF_3 to $r_m \simeq r_e$ for $CHCl_3$ to $r_m > r_e$ for $CHBr_3$, although this result should be stated with the appropriate caution, because clearly $r_m < r_e$ would also give an equivalent agreement with experiment for $CHBr_3$.

3.5. Time-Dependent Vibrational Redistribution and Separation of Time Scales. The anharmonic coupling constants, potentials, and further spectroscopic fine structures contain important information about the nature of and the time scales for intramolecular vibrational redistribution. The effective Hamiltonian and potential derived from the new observations reported here on $CHBr_3$ lead to a somewhat weaker Fermi resonance coupling ($k'_{sbb} \simeq 55$ cm^{-1}), at the lower end of the range reported before (75 ± 30 cm^{-1}).[7] This leads to a rather reduced amplitude for the very fast redistribution. This is shown in Figure 5 in terms of populations of effective Hamiltonian basis states in the $N = 6$ polyad. One observes a fast, oscillatory motion of the population of the $|v_s,v_b\rangle = |6,0\rangle$ level with a period of about 100 fs and an amplitude of 30%. Most of the exchange of population occurs with $|v_s,v_b\rangle = |5,2\rangle$. While the *rate* of redistribution is similar to what is observed in other CHX_3 molecules, the *amplitude* is by far the smallest for bromoform. This can be related to the high frequency of the stretching fundamental and the low frequency of the bending, which has also appreciable quartic anharmonicity.

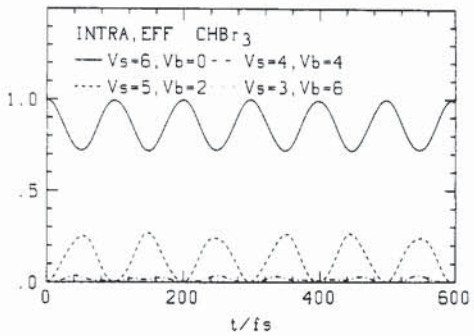

Figure 5. Time evolution of the populations of basis states $|v_s,v_b\rangle$ of the effective Hamiltonian in the $N = 6$ polyad calculated with the best fit parameters ($k'_{sbb} = 55$ cm^{-1}).

One should also consider the remaining fine structure in the N_j polyad bands, which leads to an apparently "broad" band shape in the highest overtones. Much of this is rotational structure and hot band substructure, which was already discussed in relation to Figure 2 (see also ref 7, where hot band structures are clearly resolved on several bands). This *inhomogeneous*[32] structure is not directly related to the vibrational redistribution phenomenon. Nevertheless, the total bandwidths (in the Q branch, if separate) give an estimate of the upper limit of homogeneous fine structure contributions, which are related to vibrational redistribution between the CH chromophore modes and the rovibrational modes of the heavy frame. Upper limits for homogeneous widths in 6_2 and 5_1 are 3 cm^{-1} and in 6_1 about 6 cm^{-1}. This corresponds to lower limits of lifetimes for decay into low-frequency modes of about 2 and 1 ps, respectively. When we compare this with the less than 100-fs redistribution time within the CH Fermi resonance modes, this clearly demonstrates the mode-selective nature of the redistribution and strong separation of time scales for the different processes, very similar to the situation in CHF_3, where data are more complete.[2,4]

We may mention here an interesting aspect of separation of time scales, which we have observed in some of our model calculations for parameter sets, which are "realistic", although they do not exactly correspond to the observed spectrum of $CHBr_3$. When fitting data with $F_{sbb} = F_{ssbb} = 0$ (column d) of Table VI one finds a best fit with $F_{bbbb} = -20\,605.4$ cm^{-1}. This leads to almost degenerate levels 4_5 and 3_1. The weak coupling between polyads results in substantial intensity redistribution with a separation of levels of 0.03 cm^{-1}, as observed in the variational, numerical calculations, which include interpolyad couplings. In the time domain this corresponds to an oscillation period of about 1 ns, much larger than redistribution times *within* polyads, in agreement with the effective Hamiltonian. In the final fit we have avoided the redistribution by fixing $F_{bbbb} = -20\,000$ cm^{-1}, which results in a $4_5/3_1$ level separation of 5 cm^{-1}, which totally blocks the intensity redistribution between the polyads. Of course, further interesting dynamical insights are possible from the model calculations, which we do not discuss in detail here.

(27) Ha, T. K.; Lewerenz, M.; Marquardt, R.; Quack, M. *J. Chem. Phys.* **1990**, *93*, 7097.
(28) Mecke, R. *Z. Elektrochem.* **1950**, *54*, 38.
(29) Schek, I.; Jortner, J.; Sage, M. *Chem. Phys. Lett.* **1979**, *64*, 209.
(30) Amrein, A.; Dübal, H. R.; Lewerenz, M.; Quack, M. *Chem. Phys. Lett.* **1984**, *112*, 387.
(31) Lewerenz, M.; Quack, M. *Chem. Phys. Lett.* **1986**, *123*, 197.
(32) Puttkamer von, K.; Dübal, H. R.; Quack, M. *Faraday Discuss. Chem. Soc.* **1983**, *75*, 197. Quack, M. *Philos. Trans. R. Soc. London, A* **1990**, *332*, 203.

4. Conclusions

(i) The vibrational overtone absorption spectrum of bromoform ($CHBr_3$) is dominated by bands arising from the Fermi-resonance-coupled CH stretching (ν_1) and bending (ν_4) modes, with very few and weak additional combinations with the CBr_3 stretching vibrations ν_2 and ν_5.

(ii) The tridiagonal effective Hamiltonian provides an accurate description for the assignment of band positions and intensities. The effective coupling constant $k'_{sbb} \simeq 55^{+25}_{-15}$ cm^{-1} corresponds to a strong coupling in agreement with our earlier estimate (75 ± 30 cm^{-1}), but with more adequate error bounds estimated mostly from the easily measured intensity distribution in the highest polyads (5 to 6).

(iii) The tridiagonal Fermi resonance Hamiltonian is quantitatively equivalent to variational Hamiltonians both in polar normal coordinates and curvilinear internal coordinates as shown by similarity transformations. This equivalence holds to better than experimental accuracy. Whereas the anharmonic force constants in polar normal coordinates are moderately well determined, the anharmonic constants F_{sbb} and F_{ssbb} are strongly correlated and individually undetermined even with respect to sign. This finding is similar to our earlier finding in (I), in spite of the increased size of the data set. The internal coordinate force field can be transformed to the normal-coordinate system but leads then to a very rough approximation of the accurate potential.

(iv) The possibility of pure kinetic energy coupling ($F_{ssbb} = F_{sbb} = 0$) in curvilinear coordinates can be definitely ruled out for $CHBr_3$ on the basis of the present data set, whereas the previous, smaller data set would have been consistent with such an assumption.[8] These findings for bromoform are in agreement with the findings for other CHX_3 molecules.[19]

(v) Rough estimates of band strengths and dipole functions for the CH chromophore are consistent with a systematic trend in the position of the maximum in the effective one-dimensional bond dipole moment as a function of bond extension in the series CHF_3, $CHCl_3$, and $CHBr_3$, but our present results are insufficient to prove this.[19,31]

(vi) Vibrational redistribution is found to be mode selective and very fast (≃100 fs) within the CH stretching–bending system in bromoform, but of modest amplitude even at high excitations corresponding to 6 quanta of CH stretching. Decay of the local excitation to the remaining low-frequency modes is at least an order of magnitude slower.

Our spectroscopic results may also be helpful in future interpretations of vibrational relaxation of $CHBr_3$ in the liquid on the picosecond time scale.[33] At the highest excitations there may be some interplay with chemical reaction, because the $N = 6$ polyad is above the thermodynamic threshold for the reaction $CHBr_3 \rightarrow CBr_2 + HBr$, for which a rough estimate is around 15 000 cm^{-1}, opening up possibilities of overtone-induced chemistry.

Acknowledgment. Help from Marius Lewerenz and correspondence with K. Kuchitsu is gratefully acknowledged. Our work is supported financially by the Schweizerischer Schulrat and the Schweizerischer Nationalfonds and by the U.S. National Science Foundation under (in part) the U.S.–Switzerland cooperative projects. J.D. received part of his support from the Swedish Natural Research Council.

(33) Graener, H.; Dohlus, R.; Lauberau, A. *Chem. Phys. Lett.* **1987**, *140*, 306. Graener, H. *Chem. Phys. Lett.* **1990**, *165*, 110.
(34) D'Ans-Lax. *Taschenbuch für Physiker und Chemiker*; Springer: Berlin, 1970; Band 3.

Correlation of Impact Sensitivity with Electronic Levels and Structure of Molecules

J. Sharma,† B. C. Beard,*,† and M. Chaykovsky‡

Materials Evaluation Branch and Synthesis and Formulations Branch, Naval Surface Warfare Center, 10901 New Hampshire Ave., Silver Spring, Maryland 20903-5000 *(Received: January 30, 1990; In Final Form: July 26, 1990)*

Explosive impact sensitivity among the homologous series of compounds, TNB to TATB, has been found to demonstrate a linear correlation with shake-up promotion energy. The shake-up transition observed in the N(1s) and O(1s) X-ray photoemission spectra is a direct probe of the energy separation between valence molecular orbitals at the ionized atom. Conversion of the impact energy to thermal initiation is assumed equivalent among this series of compounds due to their structural similarity, thus making the chemical reactivity the determiner of relative explosive sensitivity. TATB analogue compounds demonstrate a shake-up energy/impact sensitivity correlation with a different slope. The change in the slope is attributed to alteration in the physical coupling of impact energy due to differing structure of the analogue compounds.

Introduction

Polynitro aromatic compounds trinitrotoluene (TNT), triaminotrinitrobenzene (TATB), and hexanitrostilbene (HNS) are among the most common and most stable explosives. TATB in particular represents one of the most stable high-performance explosives known. One feature well documented for polynitro aminobenzene is the presence of shake-up structure in the X-ray induced photoelectron spectra (XPS).[1-3] A correlation has been found between the shake-up satellite peak separation from the main photoelectron line and the impact sensitivity of the compound. [This result is highly significant, demonstrating the critical role valence electronic states have in establishing macroscopic sensitivity.] In addition, this is the first report of an experimentally measured parameter that directly correlates electronic character to energetic materials sensitivity.

The first observation of a systematic variation in XPS satellite structure in the TNB/TATB family was noted a number of years ago.[4] At this time the relation to impact sensitivity was not explicitly stated, rather only the coincident variation of satellite separation with the number of electron-donating amine groups on the benzene ring. Subsequent works by Owens[5,6] and Politzer[7]

† Materials Evaluation Branch
‡ Synthesis and Formulations Branch.

(1) Pignataro, S.; Distefano, G. *J. Electron. Spectrosc. Relat. Phenom.* **1973**, *2*, 171.
(2) Pignataro, S.; Distefano, G. *Z. Naturforsch.* **1975**, *30a*, 815.
(3) Jianqi, Wang; Wenhui, Wu; Minxiu, Zeng; and Hengyuan, Lang, *J. Electron Spectrosc. Relat. Phenom.* **1988**, *46*, 363.
(4) Sharma, J.; Garrett, W. L.; Owens, F. J.; Vogel, J. L. *J. Phys. Chem.* **1982**, *86*, 1657.
(5) Owens, F. J. *J. Mol. Struct. (THEOCHEM)* **1985**, *121*, 213.